

Finite-momentum bound pairs of two electrons in an altermagnetic metal

Hui Hu,¹ Zhao Liu,¹ Jia Wang,¹ and Xia-Ji Liu¹

¹Centre for Quantum Technology Theory, Swinburne University of Technology, Melbourne 3122, Australia

(Dated: January 21, 2026)

We solve the two-electron problem on a square lattice with d -wave altermagnetism, considering both on-site and nearest-neighbor attractive interactions. The altermagnetic spin-splitting in the single-particle dispersion naturally gives rise to a ground state of two-electron bound pairs with nonzero center-of-mass momentum. This finite-momentum pairing can be interpreted as a two-body mechanism underlying the recently proposed altermagnetism-induced Fulde–Ferrell–Larkin–Ovchinnikov (FFLO) superconducting state. Additionally, when the nearest-neighbor attraction is strong, the resulting finite-momentum bound pairs exhibit a mixture of both spin-singlet and spin-triplet characteristics, suggesting the possibility of unconventional superconductors, where spin-singlet and spin-triplet pairings coexist.

I. INTRODUCTION

Exact solutions for few-particle systems often yield valuable insight into complex quantum many-body problems. A notable example is the use of the exact two-electron solution of the parent t - J model to understand bound electron pairs in the hole-rich phase of high- T_c superconductors^{1,2}, where a low-density electron superfluid may form if there is an intrinsic tendency toward pairing. Another important example comes from the exact solutions of three interacting fermions at the unitary limit (where the s -wave scattering length diverges)^{3–5}, which provide precise universal thermodynamic behavior at high temperatures through the quantum virial expansion⁶. In this work, we present the exact solutions to the two-electron problem in the presence of d -wave altermagnetism^{7–9} and show that these solutions offer a two-body perspective for understanding the recently proposed altermagnetism-induced Fulde–Ferrell–Larkin–Ovchinnikov (FFLO) superconducting state and its associated pairing symmetry^{10,11}.

Altermagnetism is a newly recognized class of magnetic order that combines key features of ferromagnetism and antiferromagnetism^{12–19}. Although the net magnetization in altermagnetic materials is zero due to their collinearly alternating spins on different sublattices, specific crystal symmetries produce a pronounced, momentum-dependent spin splitting in the electronic band structure even without an external magnetic field. As a result, altermagnets can support spin-polarized electronic bands similar to those found in ferromagnets, enabling exotic quantum phases such as FFLO superconductivity^{20–24}. This altermagnetism-driven FFLO state has been the subject of detailed studies in various contexts, including systems with purely s -wave on-site (U) and with higher-order partial-wave nearest-neighbor (V) attractive interactions^{10,11,25–34}, without or with spin-orbit coupling^{35,36}.

In the present study, we take a few-body approach to altermagnetism-induced FFLO superconductivity by exactly solving the two-electron bound-pair problem using an extended Hubbard U - V model in two dimensions. At

strong altermagnetic coupling, the two-electron continuum is significantly reshaped, developing its lowest energy at a nonzero center-of-mass momentum. As a result, the attractive interactions stabilize a ground state of two-electron bound pairs with finite momentum, providing the two-electron analog of many-electron FFLO pairing observed in altermagnetic systems. Moreover, we find that altermagnetism strongly alters the pairing symmetry of these bound pairs: they can no longer be cleanly classified as purely spin-singlet or spin-triplet, but instead generally exhibit mixed characteristics. In the many-electron case, this suggests the possible emergence of superconducting states featuring coherent superpositions of spin-singlet and spin-triplet pairings.

The remainder of the paper is organized as follows. In the next section (Sec. II), we briefly introduce the model Hamiltonian. In Sec. III, we present the two-electron ansatz and outline the method for solving the bound states below the two-electron continuum. In Sec. IV, focusing on the case of d_{xy} -wave altermagnetism, we discuss the bound-pair energy spectrum and the pairing symmetry of the associated wave functions. In Sec. V, we summarize our conclusions and discuss potential future directions. Moreover, Appendix A examines the general behavior of the whole two-electron spectrum, and Appendix B provides a concise summary of results for $d_{x^2-y^2}$ -wave altermagnetism.

II. MODEL HAMILTONIAN

We consider two electrons moving on a square lattice with the nearest-neighbor hopping strength t . In the presence of the d -wave altermagnetism, the model Hamiltonian can be written as, $\mathcal{H} = \mathcal{H}_0 + \mathcal{H}_{\text{int}}$, where for convenience the non-interacting kinetic part \mathcal{H}_0 in momentum space takes the simplest one-band form,

$$\mathcal{H}_0 = \sum_{\mathbf{k}} \left[(\varepsilon_{\mathbf{k}} + J_{\mathbf{k}}) c_{\mathbf{k}\uparrow}^\dagger c_{\mathbf{k}\uparrow} + (\varepsilon_{\mathbf{k}} - J_{\mathbf{k}}) c_{\mathbf{k}\downarrow}^\dagger c_{\mathbf{k}\downarrow} \right], \quad (1)$$

with the single-particle dispersion relation $\varepsilon_{\mathbf{k}} \equiv -2t(\cos k_x + \cos k_y)$ and the the momentum-dependent

spin-splitting $J_{\mathbf{k}}$ arising from altermagnetism. Here and in the following, $c_{\mathbf{k}\sigma}^{\dagger}$ and $c_{i\sigma}^{\dagger}$ represent the creation operators at the momentum \mathbf{k} and at the site i , respectively, for either spin-up ($\sigma = \uparrow$) or spin-down ($\sigma = \downarrow$) electrons. We will primarily focus on the case of the d_{xy} -wave altermagnetism, where $J_{\mathbf{k}}$ is given by,

$$J_{\mathbf{k}} = \lambda \sin(k_x) \sin(k_y). \quad (2)$$

The discussions on the alternative case of the $d_{x^2-y^2}$ -wave altermagnetism, where

$$J_{\mathbf{k}} = \frac{\lambda}{2} [\cos k_x - \cos k_y], \quad (3)$$

are relegated to Appendix B. To simplify the notation, throughout the paper we denote $\varepsilon_{\mathbf{k}\uparrow} = \varepsilon_{\mathbf{k}} + J_{\mathbf{k}}$ and $\varepsilon_{\mathbf{k}\downarrow} = \varepsilon_{\mathbf{k}} - J_{\mathbf{k}}$.

A. Interaction Hamiltonian

For the interaction Hamiltonian, we consider the short-range interaction potential on a $L \times L$ square lattice and use the extended Hubbard U - V model³⁷⁻³⁹, with the on-site (U) and the nearest-neighbor interaction strengths (V):

$$\mathcal{H}_{\text{int}} = \frac{U}{2} \sum_i n_i (n_i - 1) + \frac{V}{2} \sum_{i\delta} n_i n_{i+\delta}, \quad (4)$$

where $\delta = -\hat{x}, +\hat{x}, -\hat{y}, +\hat{y}$ denotes the four nearest-neighbor sites on the square lattice, and $n_i = n_{i\uparrow} + n_{i\downarrow} = \sum_{\sigma} c_{i\sigma}^{\dagger} c_{i\sigma}$ is the number of electrons on the i -th lattice site. It is readily seen that the on-site interaction occurs only between spin-up and spin-down electrons, since $n_{i\sigma}^2 = n_{i\sigma}$. In contrast, the nearest-neighbor interaction can happen between electrons with same spins. In momentum space, after the Fourier transformation we may rewrite the interaction Hamiltonian in the form^{28,40},

$$\begin{aligned} \mathcal{H}_{\text{int}} = & \frac{1}{\mathcal{S}} \sum_{\mathbf{k}, \mathbf{k}', \mathbf{q}; \sigma} V_{\mathbf{k}, \mathbf{k}', \mathbf{q}; \sigma}^{(\sigma)} c_{\mathbf{k} + \frac{\mathbf{q}}{2}, \sigma}^{\dagger} c_{-\mathbf{k} + \frac{\mathbf{q}}{2}, \sigma}^{\dagger} c_{-\mathbf{k}' + \frac{\mathbf{q}}{2}, \sigma} c_{\mathbf{k}' + \frac{\mathbf{q}}{2}, \sigma} + \\ & \frac{1}{\mathcal{S}} \sum_{\mathbf{k}, \mathbf{k}', \mathbf{q}} V_{\mathbf{k}, \mathbf{k}', \mathbf{q}}^{(\uparrow\downarrow)} c_{\mathbf{k} + \frac{\mathbf{q}}{2}, \uparrow}^{\dagger} c_{-\mathbf{k} + \frac{\mathbf{q}}{2}, \downarrow}^{\dagger} c_{-\mathbf{k}' + \frac{\mathbf{q}}{2}, \downarrow} c_{\mathbf{k}' + \frac{\mathbf{q}}{2}, \uparrow}, \end{aligned} \quad (5)$$

where $\mathcal{S} = L^2$ is the total number of the lattice sites. The two terms describe the interactions between electrons with same spin and opposite spin, respectively, with the interaction strengths^{28,40}:

$$V_{\mathbf{k}, \mathbf{k}'}^{(\sigma)} = V [\cos(k_x - k'_x) + \cos(k_y - k'_y)], \quad (6)$$

$$V_{\mathbf{k}, \mathbf{k}'}^{(\uparrow\downarrow)} = U + 2V [\cos(k_x - k'_x) + \cos(k_y - k'_y)]. \quad (7)$$

The on-site interaction is purely s -wave and does not depend on momentum, whereas the nearest-neighbor interaction exhibits significant momentum dependence. This

nearest-neighbor term can be decomposed into distinct channels (i.e., the extended s -wave, the two p -wave, and the d -wave channels), each expressible in a *separable* form. In particular, we can rewrite²⁸

$$V_{\mathbf{k}, \mathbf{k}'}^{(\uparrow\downarrow)} = \sum_{\eta=s, \text{es}, \text{p+ip}, \text{p-ip}, \text{d}} V_{\eta} f_{\eta}(\mathbf{k}) f_{\eta}^*(\mathbf{k}'), \quad (8)$$

where $V_s = U$, $V_{\text{es}} = V_{\text{p+ip}} = V_{\text{p-ip}} = V_d = V$, and the form factors of different channels are given by,

$$f_s(\mathbf{k}) = 1, \quad (9)$$

$$f_{\text{es}}(\mathbf{k}) = \cos k_x + \cos k_y, \quad (10)$$

$$f_{\text{p+ip}}(\mathbf{k}) = \sin k_x + i \sin k_y, \quad (11)$$

$$f_{\text{p-ip}}(\mathbf{k}) = \sin k_x - i \sin k_y, \quad (12)$$

$$f_d(\mathbf{k}) = \cos k_x - \cos k_y. \quad (13)$$

We can clearly identify the parity-even channel ($\eta = s, \text{es}, d$ for the spin-singlet pairing) and the parity-odd channel ($\eta = \text{p+ip}, \text{p-ip}$ for the spin-triplet pairing). In numerical calculations, to avoid the use of the complex number, it is more convenient to adopt the alternative form factors for the two p -wave channels ($\eta = p+, p-$):

$$f_{p+}(\mathbf{k}) = \sin k_x + \sin k_y, \quad (14)$$

$$f_{p-}(\mathbf{k}) = \sin k_x - \sin k_y. \quad (15)$$

It should be noted that, one can easily extend the interaction range and incorporate additional terms like next-nearest-neighbor interactions to more accurately represent a non-local interaction potential. This extension generates higher-order partial-wave components in both $V_{\mathbf{k}, \mathbf{k}'}^{(\sigma)}$ and $V_{\mathbf{k}, \mathbf{k}'}^{(\uparrow\downarrow)}$.

III. THEORETICAL FRAMEWORK

For concreteness, we focus on the case of two electrons with *opposite* spins. The same-spin scenario is less relevant here, since altermagnetism primarily alters the single-particle dispersion relation in a spin-independent way rather than affecting same-spin interactions. Therefore, only Eq. (7) contributes here.

A. Exact diagonalization of a finite lattice system

For a small lattice size L , it is convenient to diagonalize the Hamiltonian by employing the following two-electron ansatz at a given center-of-mass momentum \mathbf{Q} :

$$|\mathbf{p}\rangle \equiv c_{\mathbf{p} + \frac{\mathbf{Q}}{2}, \uparrow}^{\dagger} c_{-\mathbf{p} + \frac{\mathbf{Q}}{2}, \downarrow}^{\dagger} |\text{vac}\rangle. \quad (16)$$

It is straightforward to derive that,

$$\mathcal{H}_0 |\mathbf{p}\rangle = \left(\varepsilon_{\mathbf{p} + \frac{\mathbf{Q}}{2}, \uparrow} + \varepsilon_{-\mathbf{p} + \frac{\mathbf{Q}}{2}, \downarrow} \right) |\mathbf{p}\rangle, \quad (17)$$

$$\mathcal{H}_{\text{int}} |\mathbf{p}\rangle = \frac{1}{\mathcal{S}} \sum_{\mathbf{k}} V_{\mathbf{k}, \mathbf{p}}^{(\uparrow\downarrow)} |\mathbf{k}\rangle. \quad (18)$$

Therefore, with the complete set of the two-electron ansatz, we obtain the matrix elements of the Hamiltonian,

$$\langle \mathbf{k} | \mathcal{H} | \mathbf{p} \rangle = \delta_{\mathbf{k}\mathbf{p}} \left(\varepsilon_{\mathbf{p}+\frac{\mathbf{Q}}{2}\uparrow} + \varepsilon_{-\mathbf{p}+\frac{\mathbf{Q}}{2}\downarrow} \right) + \frac{1}{S} V_{\mathbf{k},\mathbf{p}}^{(\uparrow\downarrow)}. \quad (19)$$

By expressing the momentum within the first Brillouin zone, $\mathbf{k} = (k_x, k_y) = (n_x, n_y)2\pi/L$, where the integers n_x and n_y range from $-L/2 + 1$ to $L/2$ for an even lattice length L , we can easily diagonalize the Hamiltonian for lattice size L up to several hundred.

B. Bound states of an infinite lattice system

To treat the case of an infinite lattice, we can formulate the two-electron wave-function,

$$|\Phi\rangle = \sum_{\mathbf{p}} \Phi_{\mathbf{p}} |\mathbf{p}\rangle = \sum_{\mathbf{p}} \Phi_{\mathbf{p}} c_{\mathbf{p}+\frac{\mathbf{Q}}{2}\uparrow}^{\dagger} c_{-\mathbf{p}+\frac{\mathbf{Q}}{2}\downarrow}^{\dagger} |\text{vac}\rangle. \quad (20)$$

By using Eq. (17) and Eq. (18), one obtains,

$$\mathcal{H}_0 |\Phi\rangle = \sum_{\mathbf{p}} \left(\varepsilon_{\mathbf{p}+\frac{\mathbf{Q}}{2}\uparrow} + \varepsilon_{-\mathbf{p}+\frac{\mathbf{Q}}{2}\downarrow} \right) \Phi_{\mathbf{p}} |\mathbf{p}\rangle, \quad (21)$$

$$\mathcal{H}_{\text{int}} |\Phi\rangle = \frac{1}{S} \sum_{\mathbf{p}} \sum_{\mathbf{k}} V_{\mathbf{p},\mathbf{k}}^{(\uparrow\downarrow)} \Phi_{\mathbf{k}} |\mathbf{p}\rangle. \quad (22)$$

By projecting onto the two-electron ansatz, we rewrite the two-electron Schrödinger equation $(\mathcal{H}_0 + \mathcal{H}_{\text{int}}) |\Phi\rangle = E |\Phi\rangle$ into the standard form,

$$\left(\varepsilon_{\mathbf{p}+\frac{\mathbf{Q}}{2}\uparrow} + \varepsilon_{-\mathbf{p}+\frac{\mathbf{Q}}{2}\downarrow} \right) \Phi_{\mathbf{p}} + \frac{1}{S} \sum_{\mathbf{k}} V_{\mathbf{p},\mathbf{k}}^{(\uparrow\downarrow)} \Phi_{\mathbf{k}} = E \Phi_{\mathbf{p}}. \quad (23)$$

To solve this Schrödinger equation, it is useful to insert the separable form of the interaction potential,

$$\frac{1}{S} \sum_{\mathbf{k}\eta} V_{\eta} f_{\eta}(\mathbf{p}) f_{\eta}^*(\mathbf{k}) \Phi_{\mathbf{k}} = \left(E - \varepsilon_{\mathbf{p}+\frac{\mathbf{Q}}{2}\uparrow} - \varepsilon_{-\mathbf{p}+\frac{\mathbf{Q}}{2}\downarrow} \right) \Phi_{\mathbf{p}}. \quad (24)$$

At this point, let us introduce the variables

$$M_{\eta} \equiv \frac{1}{S} \sum_{\mathbf{k}} f_{\eta}^*(\mathbf{k}) \Phi_{\mathbf{k}}, \quad (25)$$

and solve for the wave-function,

$$\Phi_{\mathbf{p}} = \frac{\sum_{\eta} V_{\eta} f_{\eta}(\mathbf{p}) M_{\eta}}{E - \varepsilon_{\mathbf{p}+\frac{\mathbf{Q}}{2}\uparrow} - \varepsilon_{-\mathbf{p}+\frac{\mathbf{Q}}{2}\downarrow}}. \quad (26)$$

The self-consistency leads to a set of coupled equations for the variables M_{η} :

$$M_{\eta} = \frac{1}{S} \sum_{\mathbf{k}} f_{\eta}^*(\mathbf{k}) \frac{\sum_{\eta'} V_{\eta'} f_{\eta'}(\mathbf{k}) M_{\eta'}}{E - \varepsilon_{\mathbf{k}+\frac{\mathbf{Q}}{2}\uparrow} - \varepsilon_{-\mathbf{k}+\frac{\mathbf{Q}}{2}\downarrow}}. \quad (27)$$

Thus, it is useful to define,

$$L_{\eta\eta'}(E) \equiv \frac{1}{S} \sum_{\mathbf{k}} \frac{f_{\eta}^*(\mathbf{k}) f_{\eta'}(\mathbf{k})}{E - \left(\varepsilon_{\mathbf{k}+\frac{\mathbf{Q}}{2}\uparrow} + \varepsilon_{-\mathbf{k}+\frac{\mathbf{Q}}{2}\downarrow} \right)}, \quad (28)$$

and rewrite the previous coupled equations into the form,

$$\frac{(V_{\eta} M_{\eta})}{V_{\eta}} = \sum_{\eta'} [L_{\eta\eta'}(E)] (V_{\eta'} M_{\eta'}). \quad (29)$$

A non-trivial solution for the variables $V_{\eta} M_{\eta}$ requires the zero determinant³⁷,

$$\det \left[L_{\eta\eta'}(E) - \frac{\delta_{\eta\eta'}}{V_{\eta}} \right] = 0, \quad (30)$$

for a 5 by 5 matrix \mathbf{A} , where the matrix elements $A_{\eta\eta'} = L_{\eta\eta'}(E) - V_{\eta}^{-1} \delta_{\eta\eta'}$. This secular equation determines all the two-electron energy levels E , including the bound states below the threshold of the two-particle continuum (for a given center-of-mass momentum \mathbf{Q}), i.e.,

$$E < E_{2p}^{(0)}(\mathbf{Q}) = \min_{\mathbf{k}} \{ \varepsilon_{\mathbf{k}+\frac{\mathbf{Q}}{2}\uparrow} + \varepsilon_{-\mathbf{k}+\frac{\mathbf{Q}}{2}\downarrow} \}. \quad (31)$$

The eigenvectors of the matrix \mathbf{A} , upon substitution in Eq. (26), give rise to the wave-function $\Phi_{\mathbf{p}}$ up to a normalization constant.

C. Classification into the spin-singlet and spin-triplet states

In the absence of altermagnetism, the two-electron dispersion relation $E_{2p}(\mathbf{k}, \mathbf{Q}) = \varepsilon_{\mathbf{k}+\mathbf{Q}/2\uparrow} + \varepsilon_{-\mathbf{k}+\mathbf{Q}/2\downarrow}$ can be expressed as follows³⁷,

$$E_{2p}(\mathbf{k}, \mathbf{Q}) = -4t \left(\cos \frac{Q_x}{2} \cos k_x + \cos \frac{Q_y}{2} \cos k_y \right), \quad (32)$$

which is an even function in momentum \mathbf{k} . Recall that the form factors of the s -wave, extend s -wave and d -wave channels are even function of \mathbf{k} , whereas the two p -wave form factors are odd function. From this it follows that $L_{\eta\eta'} = 0$, whenever the indices η and η' belong to different parity classes. As a consequence, the two-electron wave-function have a well-defined parity. In other words, the two-electron states are purely spin-singlet or purely spin-triplet, with no admixture of singlet and triplet components.

The situation changes dramatically in the presence of altermagnetism ($\lambda \neq 0$). In this case, the two-electron dispersion relation $E_{2p}(\mathbf{k}, \mathbf{Q})$ is expressed as,

$$E_{2p}(\mathbf{k}, \mathbf{Q}) = -4t \left(\cos \frac{Q_x}{2} \cos k_x + \cos \frac{Q_y}{2} \cos k_y \right) + 2\lambda \left(\cos \frac{Q_x}{2} \sin \frac{Q_y}{2} \sin k_x \cos k_y + \sin \frac{Q_x}{2} \cos \frac{Q_y}{2} \cos k_x \sin k_y \right). \quad (33)$$

containing both even and odd components of \mathbf{k} . Thus, in general $L_{\eta\eta'}(E)$ need not vanish. As a result, all the two-electron states exhibit pairing in both the spin-singlet and spin-triplet channels. This mixed pairing character can be easily identified through the quantities M_η . For numerical analysis, it is often useful to introduce the normalized variables,

$$\tilde{M}_\eta = \frac{|M_\eta|}{\sqrt{\sum_\eta M_\eta^2}}, \quad (34)$$

which serve to characterize the dominant pairing channels of the bound pairs.

IV. RESULTS AND DISCUSSIONS

The numerical solution of the two-electron bound states using Eq. (30) is straightforward, since the integral $L_{\eta\eta'}(E)$ is well-defined for energies below the two-electron scattering continuum, i.e., $E < E_{2p}^{(0)}(\mathbf{Q})$. We have also independently examined the bound states on finite lattices with size L up to 100, and, as expected, the dependence of the bound-pair energy on lattice size is exponentially weak. In what follows, we treat separately the two scenarios in which either the on-site attraction ($U < 0$) or the nearest-neighbor attraction ($V < 0$) plays the dominant role. We concentrate on d_{xy} -wave altermagnetism and, in Appendix B, provide a brief discussion of the results for $d_{x^2-y^2}$ -wave altermagnetism.

A. The case with only attractive on-site interaction

In Fig. 1, we report the bound-pair energy E as a function of the center-of-mass momentum $\mathbf{Q} = (Q_x, Q_y)$ for an on-site attractive interaction $U = -5t$. In the presence of a d_{xy} -wave altermagnetic coupling $\lambda = 3t$, the two-dimensional (2D) contour plot in Fig. 1(a) clearly indicates that the ground-state of the bound pairs occurs at finite momentum along either the Q_x or Q_y axis. Furthermore, the one-dimensional (1D) cut along the high-symmetry Γ - X - M - Γ path in Fig. 1(b) shows that the bound-pair energy closely tracks the lower edge of the two-electron continuum $E_{2p}^{(0)}(\mathbf{Q})$ near the Γ point. As this continuum threshold also reaches a minimum at nonzero momentum, the emergence of finite-momentum bound pairs appears to directly reflect the non-trivial two-electron dispersion induced by altermagnetism.

To verify this expectation, Fig. 2 presents the bound-pair energy for two additional values of the altermagnetic coupling. For a weaker coupling ($\lambda = 2t$ in Fig.

2(a)), where the two-electron continuum exhibits its minimum at the Γ point, we indeed find that the ground-state bound pair occurs at zero center-of-mass momentum. For a stronger coupling ($\lambda = 4t$ in Fig. 2(b)), the ground-state bound pair shares exactly the same finite center-of-mass momentum at which the two-electron continuum reaches its minimum. Additionally, the binding energy E_b of the bound state, defined as $E_b = E_{2p}^{(0)}(\mathbf{Q}) - E$, generally decreases as the altermagnetic coupling increases. This behavior is anticipated, since the altermag-

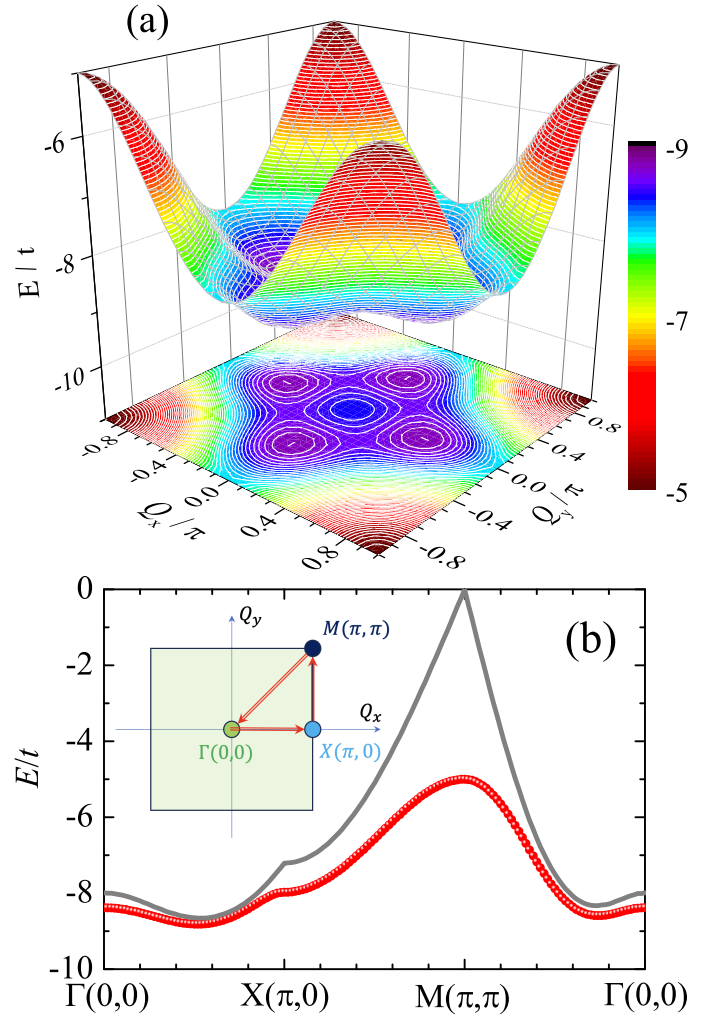


FIG. 1. The energy of the bound pairs as a function of the center-of-mass momentum $\mathbf{Q} = (Q_x, Q_y)$, at the on-site attractive interaction $U = -5t$ with the d_{xy} -wave altermagnetic coupling $\lambda = 3t$: (a) a 2D contour plot in the Q_x - Q_y plane, and (b) a 1D plot along the high-symmetry lines in the first Brillouin zone, as indicated in the inset. The grey line shows the lower bound of the two-fermion continuum $E_{2p}^{(0)}(\mathbf{Q})$. Here, we set $V = 0$.

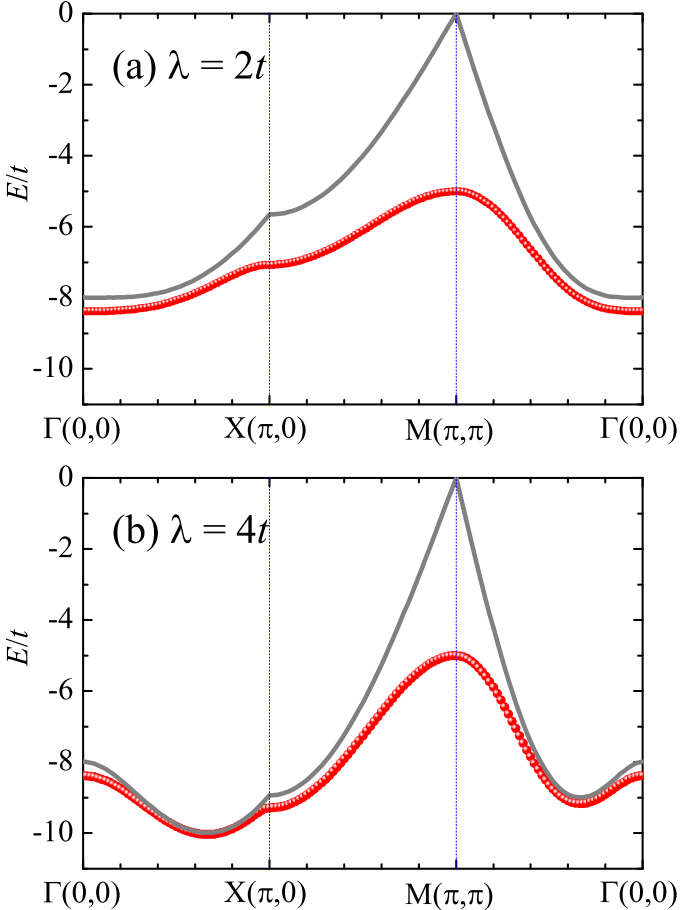


FIG. 2. The same as in Fig. 1(b), but with different d_{xy} -wave altermagnetic coupling strengths: $\lambda = 2t$ (a) and $\lambda = 4t$ (b).

netism acts effectively as a momentum-dependent magnetic field, which ultimately suppresses pairing and can break bound pairs at sufficiently large altermagnetic coupling strength.

The only exceptions to the overall decrease in binding energy are at the two high-symmetry points, Γ and M , where the binding energy remains unchanged. At these points, $J_{\mathbf{k}+\mathbf{Q}/2} = J_{-\mathbf{k}+\mathbf{Q}/2}$, so the effect of altermagnetism cancels exactly. We also note that the bound-pair energy at the M point equals the on-site interaction $U = -5t$. This corresponds to the so-called η -pairing state⁴¹, in which the two electrons form a pair on the same lattice site and are distributed in a staggered pattern throughout the whole lattice.

The finite-momentum ground state of bound pairs can be interpreted as a compelling signature of finite-momentum FFLO pairing for a many-fermion system, a phenomenon that has been widely explored in recent theoretical studies, with s -wave interaction potential. In particular, in the case of d_{xy} -wave altermagnetism, the FFLO pairing emerges when the center-of-mass momentum points along the Q_x or Q_y axis^{11,28}, mirroring the behavior of the two-electron bound state.

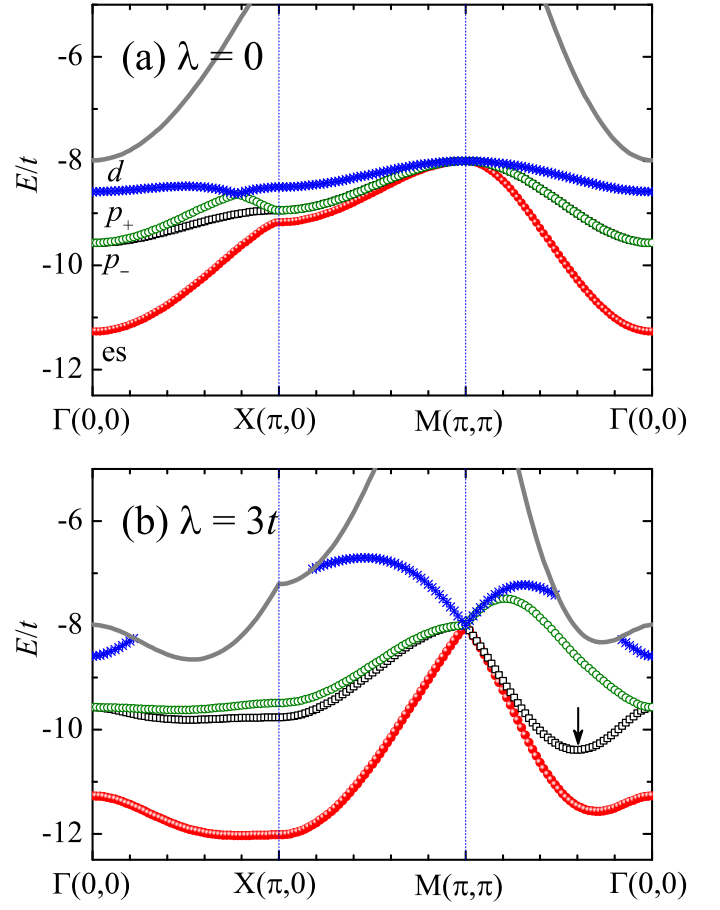


FIG. 3. The energy of the bound pairs as a function of the center-of-mass momentum $\mathbf{Q} = (Q_x, Q_y)$ along the line cut $\Gamma-X-M-\Gamma$, at the nearest-neighbor attractive interaction $V = -8t$, without (upper panel) and with the d_{xy} -wave altermagnetic coupling $\lambda = 3t$ (lower panel). Here, we take the on-site interaction $U = 2t$. The strong nearest-neighbor attraction leads to four bound states, which can be well categorized as the extended s -wave, p -wave (two-fold degenerate), and d -wave at the Γ point. The arrow in the lower panel highlights the minimum of the second lowest bound state along the Γ - M line.

B. The case with $V < 0$

In this scenario, the nearest-neighbor attractive interaction can support up to four distinct bound states³⁷. As illustrated in Fig. 3(a), without altermagnetism the four bound pairs at the Γ point can be clearly identified as extended s -wave, doubly degenerate p -wave, and d -wave states^{37,39}. Moving away from the Γ point, the energies of these different bound states may intersect at certain special momenta; however, their wave-functions $\Phi_{\mathbf{k}}$ always remain either even or odd in \mathbf{k} (not shown), which forces that the bound pairs are either spin-singlet or spin-triplet. Remarkably, at the M point all the four bound-pair energies become degenerate. This degeneracy again arises from the η -pairing mechanism discussed ear-

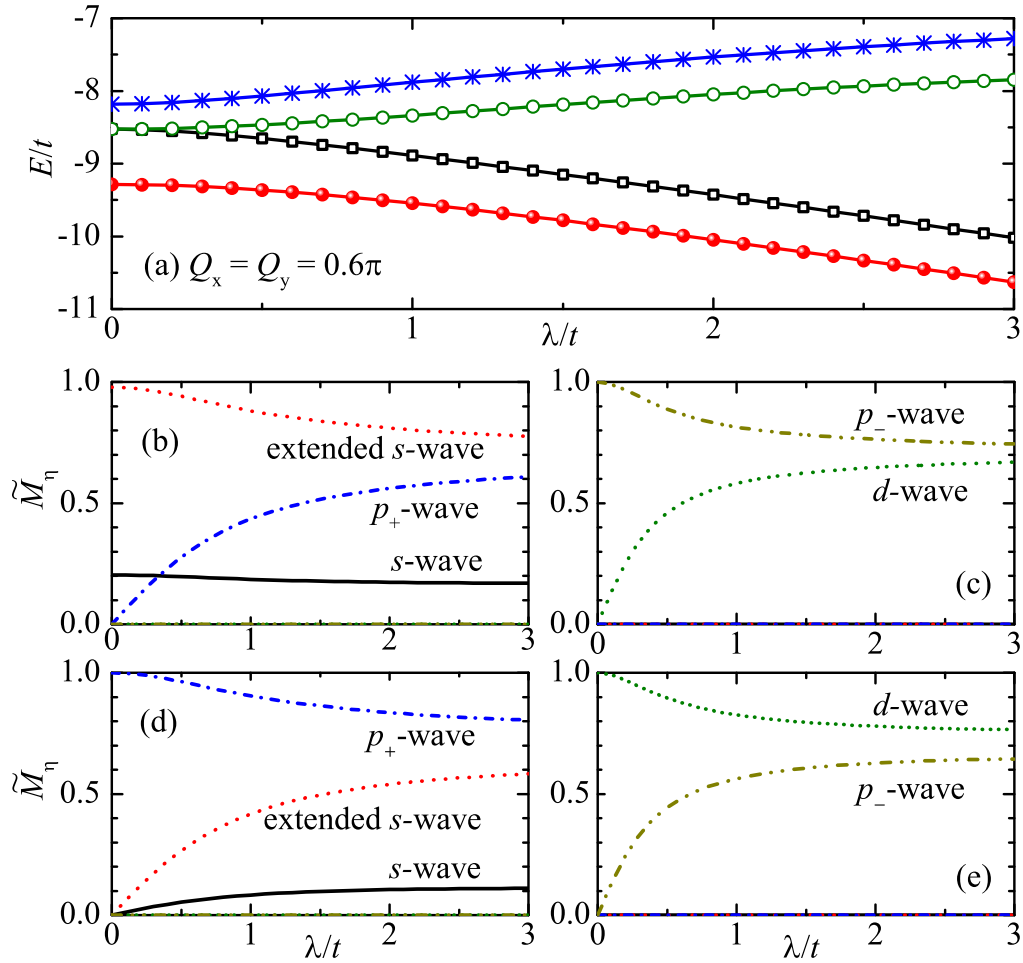


FIG. 4. (a) The energy of the bound pairs at $\mathbf{Q} = (Q_x, Q_y) = (0.6\pi, 0.6\pi)$ as a function of the d_{xy} -wave altermagnetic coupling. The two p -wave states split with increasing altermagnetic coupling. The weight of the partial-wave components (\tilde{M}_η , as explicitly indicated) of the four bound pairs: the ground-state pair (a), the first-excited pair (b), the second-excited pair (c) and the third-excited pair (d). Here, we take $U = 2t$ and $V = -8t$, as in Fig. 3.

lier: the two electrons occupy nearest-neighbor sites and pair in four different configurations, all with the same bound-state energy $E = V = -8t$.

The inclusion of an altermagnetic coupling $\lambda = 3t$ leads to several notable changes in the bound-pair dispersion. First, similar to the case of on-site attraction, the lowest bound-pair energy develops a global minimum at a finite center-of-mass momentum along the Q_x or Q_y axis, following the lower edge of the two-electron continuum. The second lowest bound-pair energy also acquires a global minimum at nonzero momentum, but along the diagonal direction (i.e., $Q_x = Q_y$ along the Γ - M line, as highlighted by the arrow in Fig. 3(b)). Therefore, in a many-electron system, one would anticipate an FFLO superconducting state with a finite center-of-mass momentum \mathbf{Q} oriented along either the x or y direction. Second, because of the pair-breaking effect of altermagnetism, we find that the fourth bound state, marked by blue stars, ceases to exist over a range of momenta. With increasing altermagnetic coupling strength, addi-

tional bound states progressively disappear (not shown). Finally and most importantly, except at the stationary Γ and M points with the highest symmetry, the bound states are no longer degenerate. In particular, the doubly degenerate p -wave states along the Γ - M line in the absence of altermagnetism are now split. As we discuss below, this splitting arises from the mixed character of the bound states: they can no longer be cleanly classified as spin-singlet or spin-triplet.

C. spin-singlet and spin-triplet mixing

In Fig. 4(a), we plot the energy splitting of the four bound pairs as a function of the altermagnetic coupling λ at a center-of-mass momentum $\mathbf{Q} = (0.6\pi, 0.6\pi)$. The corresponding evolution of the different partial-wave components for each bound state is presented in Figs. 4(b)-4(e), ordered by increasing bound-pair energy.

For the lowest bound state in Fig. 4(b), the domi-

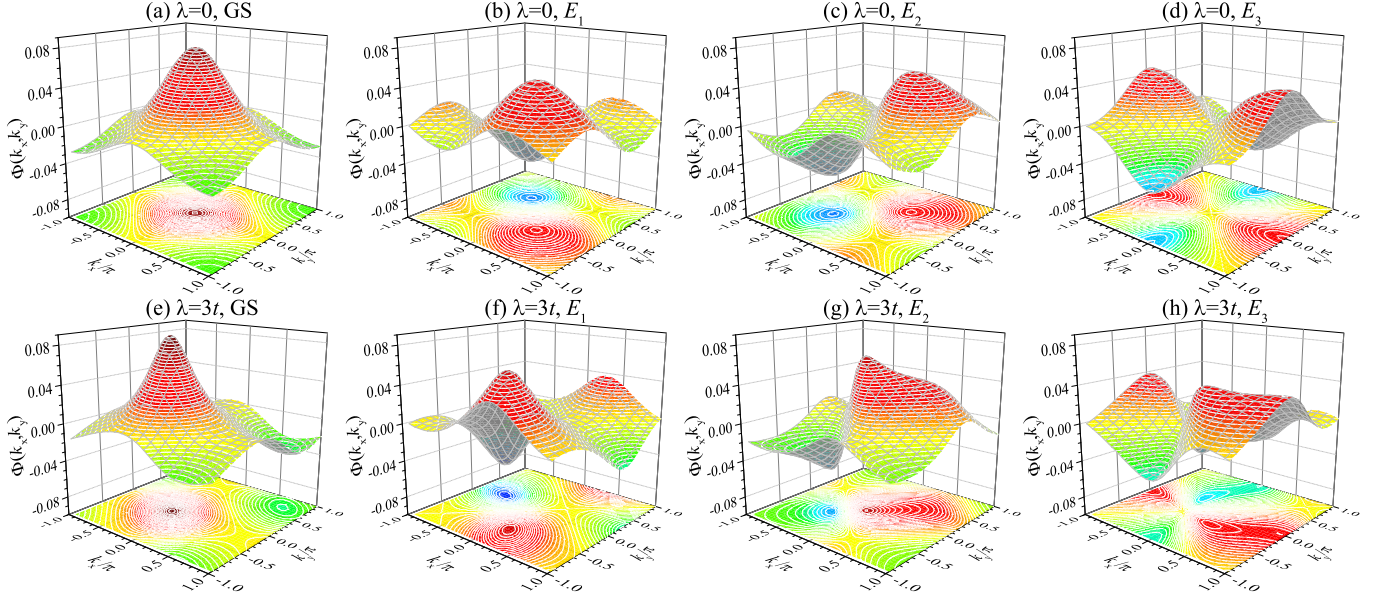


FIG. 5. The wave-functions $\Phi_{\mathbf{k}}$ of the four bound pairs at $\mathbf{Q} = (Q_x, Q_y) = (0.6\pi, 0.6\pi)$, without (upper panel) and with the d_{xy} -wave altermagnetic coupling $\lambda = 3t$ (lower panel), ordered by increasing energy. Here, we take $U = 2t$ and $V = -8t$, as in Fig. 3.

nant pairing symmetry is always the extended s -wave. As the altermagnetic coupling increases, the p_+ -wave component grows rapidly and becomes appreciable by $\lambda = 3t$. There is also a small residual s -wave contribution induced by the on-site repulsion $U = 2t$, depending only weakly on the altermagnetic coupling. Therefore, the ground-state bound pair clearly forms a coherent superposition of spin-singlet (extended s -wave) and spin-triplet (p_+ -wave) components. Analogous to bonding and anti-bonding molecular states, this superposition implies the existence of a complementary anti-bond state in which the roles of the extended s -wave and p_+ -wave components are reversed. From Fig. 4(d), we see that this anti-bond state is exactly given by the third lowest bound pair, where the state that was initially p_+ -wave dominated evolves, at sufficiently strong altermagnetic coupling, into a nearly equal-weight superposition of p_+ -wave and extended s -wave. Similarly, Fig. 4(c) and Fig. 4(e) show that the second and fourth bound pairs correspond to the bonding and anti-bonding combinations of the p_- -wave and d -wave components, respectively.

The mixed character of the bound pairs is most clearly seen in their pairing wave-function $\Phi_{\mathbf{k}}$, as reported in Fig. 5. In the absence of altermagnetism (see the upper panel), each momentum-space wave-function exhibits a well-defined symmetry: extended s -wave, p -wave or d -wave symmetry, with increasing bound-state energy. By contrast, introducing the altermagnetic coupling $\lambda = 3t$ substantially alters the momentum distribution of each wave-function, breaking rotational symmetry. For instance, in the ground-state bound pair illustrated in Fig. 5(e), the wave-function maximum shifts away from the origin and a pronounced minimum emerges near the cor-

ner of first Brillouin zone at the M point, reflecting the admixture of the p -wave component.

It is worth noting that, at $\mathbf{Q} = (Q_x, Q_y) = (0.6\pi, 0.6\pi)$ there is a mirror symmetry m_d along the diagonal $k_x = k_y$. Under this symmetry, the s -wave, extended s -wave, and p_+ -wave channels are even, while the p_- -wave and d -wave channels are odd. As $E_{2p}(\mathbf{k}, \mathbf{Q})$ remains unchanged under the exchange $k_x \leftrightarrow k_y$ when $Q_x = Q_y$ (see Eq. (33)), only pairing channels with the same mirror parity can hybridize. Consequently, the s -wave, extended s -wave, and p_+ -wave components can mix with one another, as shown in Fig. 4(b) and Fig. 4(d), and similarly the p_- -wave and d -wave channels mix among themselves.

The observed singlet-triplet mixing is expected to have significant consequences for the finite-momentum FFLO superconducting state that may emerge in a many-electron system. In that context, the many-particle pairing predominantly occurs near the Fermi surface. At low electron densities (or small lattice filling factor), one can anticipate that the order parameter will involve a mixture of extended s -wave and p_+ -wave pairings. At higher electron densities, the presence of Fermi surface and the Pauli exclusion principle suppress pairing at small relative momenta, making a mixed d -wave and p_- -wave pairing more likely to characterize the order parameter.

V. CONCLUSIONS AND OUTLOOKS

In summary, we have obtained an exact solution for two-electron bound pairs in an altermagnetic metal on a square lattice, considering both on-site and nearest-neighbor attractive interactions. The altermagnetic cou-

pling strongly alters the threshold of the two-electron scattering continuum, producing a global minimum at finite center-of-mass momentum when the coupling is sufficiently strong. The bound-pair energy closely follows this modified continuum threshold, so that the ground state of the bound pairs can occur at nonzero center-of-mass momentum regardless of the form of the interaction. This finite-momentum bound pair can be naturally interpreted as the two-electron mechanism underpinning the recently proposed altermagnetism-driven FFLO superconducting state.

By analyzing the relative wave function of bound pairs in momentum space, we have further found that for a nearest-neighbor attraction capable of supporting multiple partial-wave interactions, the finite-momentum bound states exhibit a mixed pairing symmetry. Consequently, in a many-electron system one should expect an FFLO order parameter with a mixed singlet-triplet character. Notably, a recent mean-field study has indeed reported such mixed singlet-triplet finite-momentum pairing with both d -wave and p -wave components³⁴, in the presence of altermagnetism and nearest-neighbor attraction. A comprehensive investigation of the pairing instability in many-electron systems could be pursued in future work using the well-established Thouless criterion under the ladder approximation within the many-body T -matrix approach^{42,43}.

ACKNOWLEDGMENTS

This research was supported by the Australian Research Council's (ARC) Discovery Program, Grants Nos. DP240101590 (H.H.), FT230100229 (J.W.) and DP240100248 (X.-J.L.).

Appendix A: The spectrum of all the two-electron energy levels

In Fig. 6, we show the complete two-electron spectrum along the Γ - X - M - Γ path, including both on-site and nearest-neighbor interactions. For sufficiently strong interactions, five bound states always appear, due to the existence of the five distinct partial-wave channels. The sign of the interaction does not affect this: attractive interactions produce bound pairs at the bottom of the spectrum, while repulsive interactions produce bound pairs at the top. At equal magnitudes of interaction strength, the attractive and repulsive bound states are symmetrically positioned about $E = 0$, reflecting the particle-hole symmetry of the single-particle dispersion $\varepsilon_{\mathbf{k}}$.

Appendix B: The case of $d_{x^2-y^2}$ altermagnetism

Here, we briefly summarize the behavior of bound pairs in the presence of $d_{x^2-y^2}$ -wave altermagnetism, where

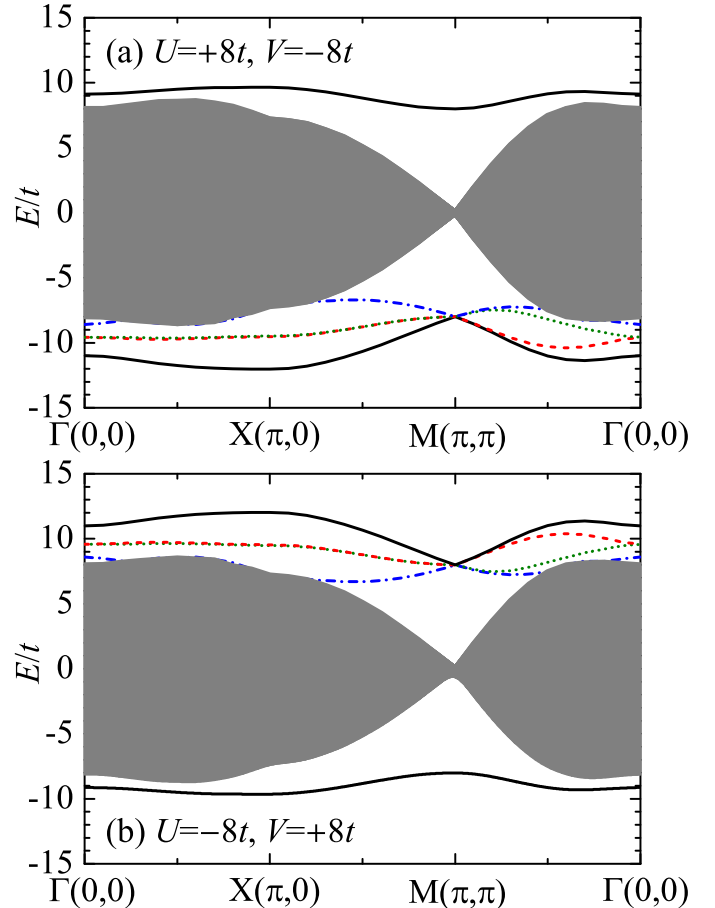


FIG. 6. The energy-level diagrams of two interacting fermions with unlike spin. In the presence of the large on-site interaction U and nearest-neighbor interaction V , there are in general five bound pairs, either at the bottom (for attractive interactions) or at the top (for repulsive interactions) of the two-fermion continuum, which are illustrated in grey. Here, we take a d_{xy} -wave altermagnetic coupling $\lambda = 3t$.

$J_{\mathbf{k}} = \lambda(\cos k_x - \cos k_y)/2$. In this case, the altermagnetic coupling $\lambda = 4t$ turns out to be a critical coupling constant, at which the single-particle dispersions for spin-up and spin-down electrons becomes $\varepsilon_{\mathbf{k}\uparrow} = -4t \cos(k_y)$ and $\varepsilon_{\mathbf{k}\downarrow} = -4t \cos(k_x)$, respectively. It is then straightforward to see that the lower edge of the two-electron continuum becomes flat, i.e., $E_{2p}^{(0)}(\mathbf{Q}) = -4t$, regardless of the center-of-mass momentum \mathbf{Q} .

In Fig. 7, we report the bound-pair energies for two $d_{x^2-y^2}$ -wave altermagnetic coupling strengths, $\lambda = 3t$ (upper panel) and $\lambda = 5t$ (lower panel). Once $\lambda > 4t$, a global minimum develops at the M point in the lower edge of the two-electron continuum, supporting finite-momentum bound pairs at the same M point. In a many-electron system, we anticipate the possible formation of a finite-momentum FFLO-type order parameter. However, because of many-particle correlation, the center-of-mass momentum is not necessarily pinned to the M point $\mathbf{Q} = (\pi, \pi)$.

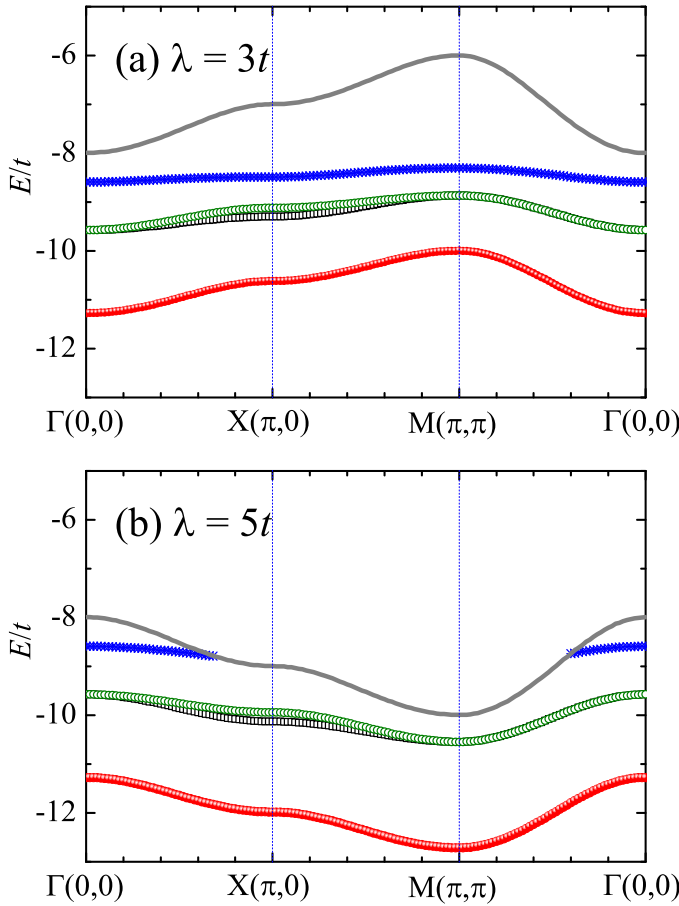


FIG. 7. The energy of the bound pairs as a function of the center-of-mass momentum $\mathbf{Q} = (Q_x, Q_y)$ along the line cut Γ - X - M - Γ , at the nearest-neighbor attractive interaction $V = -8t$, with the $d_{x^2-y^2}$ -wave altermagnetic coupling $\lambda = 3t$ (a) and $\lambda = 5t$ (b). Here, we take the on-site interaction $U = 2t$.

¹ H. Q. Lin, Dilute gas of electron pairs in the t - J model, Phys. Rev. B **44**, 4674 (1991).

² A. G. Petukhov, J. Galán, and J. A. Vergés, Bound states of two electrons described by the t - J model, Phys. Rev. B **46**, 6212 (1992).

³ X.-J. Liu, H. Hu, and P. D. Drummond, Virial Expansion for a Strongly Correlated Fermi Gas, Phys. Rev. Lett. **102**, 160401 (2009).

⁴ X.-J. Liu, H. Hu, and P. D. Drummond, Three attractively interacting fermions in a harmonic trap: Exact solution, ferromagnetism, and high-temperature thermodynamics, Phys. Rev. A **82**, 023619 (2010).

⁵ X.-J. Liu, H. Hu, and P. D. Drummond, Exact few-body results for strongly correlated quantum gases in two dimensions, Phys. Rev. B **82**, 054524 (2010).

⁶ H. Hu, P. D. Drummond, and X.-J. Liu, Universal thermodynamics of strongly interacting Fermi gases, Nature Phys. **3**, 469 (2007).

⁷ L. Šmejkal, J. Sinova, and T. Jungwirth, Emerging Research Landscape of Altermagnetism, Phys. Rev. X **12**, 040501 (2022).

⁸ T. Jungwirth, R. M. Fernandes, E. Fradkin, A. H. MacDonald, J. Sinova, and L. Šmejkal, Altermagnetism: an unconventional spin-ordered phase of matter, *Newton* **1**, 100162 (2025).

⁹ Z. Liu, H. Hu, and X.-J. Liu, Altermagnetism and superconductivity: A short historical review, arXiv:2510.09170 (2025).

¹⁰ S.-B. Zhang, L.-H. Hu, and T. Neupert, Finite-momentum Cooper pairing in proximitized altermagnets, Nat. Commun. **15**, 1801 (2024).

¹¹ H. Hu, Z. Liu, and X.-J. Liu, Unconventional superconductivity of an altermagnetic metal: Polarized BCS and inhomogeneous FFLO states, Phys. Rev. B **112**, 184501 (2025).

¹² Y. Noda, K. Ohno, and S. Nakamura, Momentum-dependent band spin splitting in semiconducting MnO_2 : a density functional calculation, Phys. Chem. Chem. Phys. **18**, 13294 (2016).

¹³ M. Naka, S. Hayami, H. Kusunose, Y. Yanagi, Y. Motome,

and H. Seo, Spin current generation in organic antiferromagnets, *Nat. Commun.* **10**, 4305 (2019).

¹⁴ S. Hayami, Y. Yanagi, and H. Kusunose, Momentum-Dependent Spin Splitting by Collinear Antiferromagnetic Ordering, *J. Phys. Soc. Jpn.* **88**, 123702 (2019).

¹⁵ K.-H. Ahn, A. Hariki, K.-W. Lee, and J. Kuneš, Antiferromagnetism in RuO_2 as d -wave Pomeranchuk instability, *Phys. Rev. B* **99**, 184432 (2019).

¹⁶ S. Hayami, Y. Yanagi, and H. Kusunose, Bottom-up design of spin-split and reshaped electronic band structures in antiferromagnets without spin-orbit coupling: Procedure on the basis of augmented multipoles, *Phys. Rev. B* **102**, 144441 (2020).

¹⁷ L. Šmejkal, R. González-Hernández, T. Jungwirth, and J. Sinova, Crystal time-reversal symmetry breaking and spontaneous Hall effect in collinear antiferromagnets, *Sci. Adv.* **6**, eaaz8809 (2020).

¹⁸ I. I. Mazin, Altermagnetism in MnTe: Origin, predicted manifestations, and routes to detwinning, *Phys. Rev. B* **107**, L100418 (2023).

¹⁹ O. J. Amin, A. Dal Din, E. Golias, Y. Niu, A. Zakharov, S. C. Fromage, C. J. B. Fields, S. L. Heywood, R. B. Cousins, F. Maccherozzi, J. Krempaský, J. H. Dil, D. Kriegner, B. Kiraly, R. P. Campion, A. W. Rushforth, K. W. Edmonds, S. S. Dhesi, L. Šmejkal, T. Jungwirth, and P. Wadley, Nanoscale imaging and control of altermagnetism in MnTe, *Nature* **636**, 348 (2024).

²⁰ P. Fulde and R. A. Ferrell, Superconductivity in a Strong Spin-Exchange Field, *Phys. Rev.* **135**, A550 (1964).

²¹ A. I. Larkin and Yu. N. Ovchinnikov, Nonuniform state of superconductors, *Zh. Eksp. Teor. Fiz.* **47**, 1136 (1964) [Sov. Phys. JETP **20**, 762 (1965)].

²² R. Casalbuoni and G. Nardulli, Inhomogeneous superconductivity in condensed matter and QCD, *Rev. Mod. Phys.* **76**, 263 (2004).

²³ H. Hu and X.-J. Liu, Mean-field phase diagrams of imbalanced Fermi gases near a Feshbach resonance, *Phys. Rev. A* **73**, 051603(R) (2006).

²⁴ H. Hu, X.-J. Liu, and P. D. Drummond, Phase Diagram of a Strongly Interacting Polarized Fermi Gas in One Dimension, *Phys. Rev. Lett.* **98**, 070403 (2007).

²⁵ S. Sumita, M. Naka, and H. Seo, Fulde-Ferrell-Larkin-Ovchinnikov state induced by antiferromagnetic order in κ -type organic conductors, *Phys. Rev. Res.* **5**, 043171 (2023).

²⁶ D. Chakraborty and A. M. Black-Schaffer, Zero-field finite-momentum and field-induced superconductivity in altermagnets, *Phys. Rev. B* **110**, L060508 (2024).

²⁷ Y. Fukaya, B. Lu, K. Yada, Y. Tanaka, and J. Cayao, Superconducting phenomena in systems with unconventional magnets, *J. Phys.: Condens. Matter* **37**, 313003 (2025).

²⁸ S. Hong, M. J. Park, and K.-M. Kim, Unconventional p -wave and finite-momentum superconductivity induced by altermagnetism through the formation of Bogoliubov Fermi surface, *Phys. Rev. B* **111**, 054501 (2025).

²⁹ I. V. Iorsh, Electron pairing by dispersive phonons in altermagnets: Reentrant superconductivity and continuous transition to finite momentum superconducting state, *Phys. Rev. B* **111**, L220503 (2025).

³⁰ G. Sim and J. Knolle, Pair Density Waves and Supercurrent Diode Effect in Altermagnets, *Phys. Rev. B* **112**, L020502 (2025).

³¹ S. Sumita, M. Naka, and H. Seo, Phase-modulated superconductivity via altermagnetism, *Phys. Rev. B* **112**, 144510 (2025).

³² H. Hu and X.-J. Liu, Quantum Lifshitz points in an altermagnetic superconductor, *AAPPS Bull.* **35**, 35 (2025).

³³ Z. Liu, H. Hu, and X.-J. Liu, Fulde-Ferrell-Larkin-Ovchinnikov states and topological Bogoliubov Fermi surfaces in altermagnets: an analytical study, arXiv:2508.07813.

³⁴ K. Jasiewicz, P. Wójcik, M. Nowak, and M. Zegrodnik, Interplay between altermagnetism and superconductivity in two dimensions: intertwined symmetries and singlet-triplet mixing, arXiv:2511.05190.

³⁵ V. S. de Carvalho and H. Freire, Unconventional superconductivity in altermagnets with spin-orbit coupling, *Phys. Rev. B* **110**, L220503 (2024).

³⁶ K. Mukasa and Y. Masaki, Finite-momentum Superconductivity in Two-dimensional Altermagnets with a Rashba-type Spin–Orbit Coupling, *J. Phys. Soc. Jpn.* **94**, 064705 (2025).

³⁷ P. Kornilovitch, Enhanced stability of bound pairs at nonzero lattice momenta, *Phys. Rev. B* **69**, 235110 (2004).

³⁸ P. Kornilovitch, Ferromagnetism and Borromean Binding in Three-Fermion Clusters, *Phys. Rev. Lett.* **112**, 077202 (2014).

³⁹ P. Kornilovitch, Two-particle bound states on a lattice, *Ann. Phys. (N. Y.)* **460**, 169574 (2024).

⁴⁰ D. Zhu, Z.-Y. Zhuang, Z. Wu, and Z. Yan, Topological superconductivity in two-dimensional altermagnetic metals, *Phys. Rev. B* **108**, 184505 (2023).

⁴¹ C. N. Yang, η pairing and off-diagonal long-range order in a Hubbard model, *Phys. Rev. Lett.* **63**, 2144 (1989).

⁴² D. J. Thouless, Perturbation theory in statistical mechanics and the theory of superconductivity, *Ann. Phys. (N. Y.)* **10**, 553 (1960).

⁴³ X.-J. Liu and H. Hu, BCS-BEC crossover in an asymmetric two-component Fermi gas, *Europhys. Lett.* **75**, 364 (2006).